Structural Properties of Chemically Synthesized Nanostructured Ni and Ni:Ni_3C Nanocomposites

Diandra L. Leslie-Pelecky,*,† X. Q. Zhang,‡ S. H. Kim,‡ M. Bonder,† and Reuben D. Rieke‡

Department of Physics & Astronomy and Center for Materials Research & Analysis, University of Nebraska, Lincoln, Nebraska 68588-0111, and Department of Chemistry and Center for Materials Research & Analysis, University of Nebraska, Lincoln, Nebraska 68588-0304

Received May 7, 1997. Revised Manuscript Received October 13, 1997[⊗]

We have used a reductive technique known to produce highly reactive metals to fabricate nickel and nickel-based nanostructured materials. The strong dependence of the magnetic, chemical, electrical, and optical properties of nanostructured materials are intimately correlated with material structure; thus, thorough knowledge of the effect of synthesis parameters on the structure is critical for the refinement of fabrication techniques. X-ray diffraction and electron microscopy are used to determine the effect of the synthetic conditions and subsequent processing on the material structure. Characteristic lengths of these materials range from 3 to 50 nm, depending on synthesis and annealing conditions. Annealing produces a metastable Ni_3C phase that forms only in the presence of active carbon, suggesting that not only active nickel but also active carbon results from this process. The addition of $P(Ph)_3$ affects the time and temperature dependence of the nickel crystallite growth, the temperature at which Ni_3C crystallites are first observed and the maximum temperature to which Ni_3C can be retained.

Introduction

Nanostructured materials often have unique electrical, chemical, structural, and magnetic properties due to a combination of reduced grain size and large surface or interface areas relative to bulk materials.[1−4] Applications may include information storage, color imaging, bioprocessing, catalysis, magnetic refrigeration, ferrofluids, hard coatings, and improved manufacturing of brittle materials. This paper examines the correlation between the synthetic process and resulting structural characteristics of nickel-based nanostructures fabricated using chemical reduction. The exceptional reactivity of the particles allows the production of unique nanocomposite materials containing both nickel and Ni_3C. Triphenyl phosphine ($P(Ph)_3$) is used to control the formation, growth, and decomposition of the metastable Ni_3C phase.

Synthesis and processing of nanostructured materials have been reviewed by several authors.[1,5,6] Common techniques include inert gas condensation,[7] microemulsion or inverse micelle synthesis,[8−10] carbon arc techniques,[11] sputtering,[12−14] molecular self-assembly,[15] chemical reduction,[16−18] metal vapor trapping,[19−21] sonochemical techniques,[22] mechanical alloying,[23] and partial annealing of quenched materials[24−26] among others.

In 1972, Rieke and co-workers reported a general approach for preparing highly reactive metal powders

[⊗] Abstract published in *Advance ACS Abstracts,* December 1, 1997.

(1) Eastman, J.; Siegel, R. W. *Nanophase Synthesis Assembles Materials from Atomic Clusters*; Eastman, J., Siegel, R. W., Eds.; 1989; January, p 56.
(2) Siegel, R. W. *Nanostruct. Mater.* **1994**, *4*, 121.
(3) Gleiter, H. *Mater. Sci. Forum* **1995**, *189−190*, 67.
(4) Gryaznov, V. G.; Trusov, L. I. *Prog. Mater. Sci.* **1993**, *37*, 289.
(5) Leslie-Pelecky, D. L.; Rieke, R. D. *Chem. Mater.* **1996**, *8*, 1770−1783.
(6) Siegel, R. W., Siegel, R. W., Eds.; Kluwer Academic Publishers: Dordrecht, 1993.
(7) Yiping, L.; Hadjipanayis, G. C.; Sorensen, C. M.; Klabunde, K. J. *J. Appl. Phys.* **1994**, *75*, 5885.
(8) Chen, J. P.; Sorenson, C. M.; Klabunde, K. J.; Hadjipanayis, G. C. *Phys. Rev. B* **1995**, *51*, 11527.
(9) Lin, H.-M.; Hsu, C. M.; Yao, Y. D.; Chen, Y. Y. *Nanostruct. Mater.* **1998**, *6*, 977.
(10) Venturini, E. L.; Wilcoxon, J. P.; Newcomer, P. P. *Mater. Res. Soc. Sump. Proc* **1994**, *351*, 311.
(11) Scott, J. H.; Majetich, S. A. *Phys. Rev. B* **1995**, *52*, 12564.
(12) Falicov, L. M.; Pierce, D. T.; Bader, S. D.; Gronsky, R.; Hathaway, K. B.; Hopster, H. J.; Lambeth, D. N.; Parkin, S. S. P.; Prinz, G.; Salamon, M.; Schuller, I. K.; Victora, R. H. *J. Mater. Res* **1990**, *5*, 1299.
(13) Childress, J. R.; Chien, C. L.; Nathan, M. *Appl. Phys. Lett.* **1989**, *56*, 95.
(14) Ambrose, T.; Gavrin, A.; Chien, C. L. *J. Magn. Magn. Mater.* **1992**, *116*, L311.
(15) Singh, A.; Markowitz, M.; Chow, G. M. *Nanostruct. Mater.* **1995**, *5*, 141.
(16) Rieke, R. D. *Crit. Rev. Surf. Chem.* **1991**, *1*, 131.
(17) Wonterghen, J. v.; Mørup, S.; Koch, C. J. W.; Charles, S. W.; Wells, S. *Nature* **1986**, *322*, 622.
(18) Glavee, G. N.; Klabunde, K. J.; Sorensen, C. C.; Hadjipanayis, G. C. *Inorg. Chem.* **1995**, *34*, 28.
(19) Kernizan, C. F.; Klabunde, K. J.; Sorensen, C. M.; Hadjipanayis, G. C. *Chem. Mater.* **1990**, *2*, 70.
(20) Hooker, P.; Tan, B. J.; Klabunde, K. J.; Suib, S. *Chem. Mater.* **1991**, *3*, 947.
(21) Hooker, P. D.; Klabunde, K. J. *Chem. Mater.* **1993**, *5*, 1089.
(22) Suslick, K. S. *MRS Bull.* **1995**, *April*, 29.
(23) Koch, C. C.; Shull, R. D.; Sanchez, J. M. *Nanophases and Nanocrystalline structured*; Shull, Sanchez, Eds.; 1994; p 19.
(24) Lu, K. *Phys. Rev. B* **1995**, *51*, 18.
(25) Herzer, G. *J. Magn. Magn. Mater.* **1996**, *157/158*, 133−136.
(26) Krönmuller, H.; Schrefl, T. *J. Magn. Magn. Mater.* **1994**, *129*, 66.

S0897-4756(97)00297-4 CCC: $15.00
Published on Web 01/19/1998

by reducing metal salts in ethereal or hydrocarbon solvents using alkali metals.[27−29] High reactivity, for the most part, refers to oxidative−addition reactions. Since the initial report, several other reduction methods have been reported,[30−32] including metal−graphite compounds,[33] magnesium-anthracene complexes, and dissolved alkalides.[34,35] The Rieke technique has the advantage of requiring minimal specialized equipment and the ability to produce large quantities of material at a single time.

Both the Rieke process and the solvated metal atom dispersion method (SMAD)[36] produce highly active macroscopic metal particles with nanometer grain sizes. A consequence of the particles' high reactivity is the inclusion of hydrocarbon fragments during synthesis. Although both techniques produce particles having large surface areas, the Rieke metals are more reactive in oxidative−addition reactions than the SMAD metal slurries, suggesting that factors such as the absorption of anions generated from solvent cleavage during reduction, the alkali salts generated or both may facilitate electron transfer in the rate-limiting step. High densities of dislocations and imperfections may also accelerate reaction rates. The Rieke approach has been used to prepare highly reactive Mg, Zn, Al, In, Th, U, Tl, Cr, Mn, Fe, Ni, Co, Cd, Pt, Pd, and Ca.

Experimental Procedure

Variations in the synthetic process can affect the nanostructure and thus the chemical and magnetic properties of nanostructured materials. Nickel was chosen due to our interest in its magnetic properties[5,37] and its industrial importance as a catalyst. The materials discussed in this paper involve reductions of the form

$$NiX_2 + 2Li \xrightarrow{\text{electron carrier}} Ni^* + 2LiX \qquad (1)$$

where X is Br or Cl. Reductions are carried out under an argon atmosphere in a solvent in which both lithium and the starting salt are at least partially soluble. The electron carrier, naphthalene, is used in molar concentrations from 10% to 100% of the lithium. The alkali salt (LiX) generated in the reduction can be removed by washing the product with an appropriate solvent after synthesis. Variable parameters include type of starting salt, solvent, concentration of electron carrier, and type of washing solvent (if any).

For all samples, Linde prepurified-grade argon was further purified by passage over a BASF R3-11 catalyst column at 150 °C, a phosphorus pentoxide column, and a column of granular potassium hydroxide. Toluene was distilled from Na/K alloy under an argon atmosphere immediately before use. Tetramethylethylenediamine (TMEDA) and triphenylphosphine (PPh_3) were used without further purification.

Run 38. Lithium (0.139 g, 21 mmol), naphthalene (0.256 g, 2 mmol), and nickel bromide (2.185 g, 10 mmol) were weighed and charged in a reaction flask under argon in a drybox (Vacuum Atmospheres Co.). The reaction flask was hooked up to a dual-manifold vacuum/argon system. Toluene (25 mL) and TMEDA (2.28 g, 21 mmol) were syringed into the reaction flask at room temperature. The resulting mixture was stirred at room temperature overnight. The newly formed nickel slurry (black powder) was allowed to settle, and the supernatant was drawn off via cannula. The nickel slurry was washed with freshly distilled toluene (25 mL) and TMEDA (2.28 g) and the supernatant removed via cannula. The washing step was repeated for a total of five times. Drying of the slurry (in vacuum) produced 0.81 g of active nickel, a yield of 138% based on the amount of nickel bromide used.

Run 91. Run 91 was completed using the same procedure as run 38, except that the slurry was washed seven times instead of five times before drying. The yield was 100%, based on nickel bromine. Although the same apparatus was used for both runs 38 and 91, extra care was taken in run 91 to maintain the integrity of the vacuum/argon manifold due to concerns about the introduction of oxygen in run 38.

Run 39. Run 39 was prepared using the same procedure described for run 38, except that triphenylphosphine (PPh_3) was added with the lithium, naphthalene and nickel bromide prior to the start of the reaction. The yield was 113% based on nickel bromide.

Run 92. Run 92 was prepared using the same procedure as used for run 38, except that the triphenylphosphine was added after the nickel slurry was formed. The resulting mixture was stirred overnight and then washed seven times as previously described. The yield was 130% based on nickel bromide.

A unique feature of this synthetic technique is that if the washing step is eliminated, metal particles embedded in a LiBr or LiCl matrix can be produced. When the alkali salt is hygroscopic, the presence of the salt may provide an in situ getter to protect the metal particles from oxidation.

X-ray diffraction (XRD) measurements were performed on a Rigaku D-Max B diffractometer using Cu Kα radiation. The diffracting crystallite size (DCS) is obtained using the Scherrer technique, in which the breadth, B, of a diffraction peak located at 2θ is related to the crystallite size by

$$\mathrm{DCS} = \frac{0.9\lambda}{B\cos\theta} \qquad (2)$$

where λ is the X-ray wavelength. We have specifically adopted the terminology of diffracting crystallite size (DCS) to distinguish the quantity obtained from eq 2 from overall particle size. XRD measurements are made by placing the particles in a small amount of silicone grease on the surface of a zero-background quartz holder. An estimate of the relative amounts of nickel and other compounds present is obtained from the ratio of the areas under the corresponding peaks. Scanning electron microscopy (SEM) and transmission electron microscopy (TEM) provide structural information. Energy-dispersive X-ray spectroscopy (EDX) provides a qualitative identification of chemical composition.

Results

The utility of the synthetic technique is demonstrated by the physical and chemical characteristics of the resulting particles, which are significantly different than commercially available powders. Scanning electron microscopy (SEM) and transmission electron microscopy (TEM) indicate particle sizes from microns to nanometers, depending on the specific preparation technique and annealing conditions. Figure 1 shows that, on a scale of microns, these metals have a spongelike characteristic, in contrast to the smooth surfaces of com-

(27) Rieke, R. D. *Acc. Chem. Res.* **1977**, *10*, 301.
(28) Rieke, R. D. *Top. Curr. Chem.* **1975**, *59*, 1.
(29) Burns, T. P.; Rieke, R. D. *J. Org. Chem* **1987**, *52*, 3674.
(30) Csuk, R.; Glanzer, B. L.; A. Furstner *Adv. Organomet. Chem.* **1988**, *28*, 85.
(31) Savoia, D.; Tombini, C.; Umani-Ronchi, A. *Pure Appl. Chem.* **1985**, *57*, 1977.
(32) Bogdanovic, B. *Acc. Chem. Res.* **1988**, *21*, 261.
(33) Marceau, P.; Gautreau, L.; F. Beguin *J. Organomet. Chem.* **1991**, *403*, 21.
(34) Tsai, K. L.; Dye, J. *Faraday Discuss. Chem. Soc.* **1991**, *92*, 45.
(35) Tsai, K.-L.; Dye, J. *J. Am. Chem. Soc.* **1991**, *113*, 1650.
(36) Klabunde, K. J.; Cardenas-Trivino, G. *Metal Atom/Vapor Approaches to Active Metal Clusters/Particles*; Klabunde, K. J., Cardenas-Trivino, G., Ed.; VCH: New York, 1996; pp 237−278.
(37) Leslie-Pelecky, D. L.; Zhang, X. Q.; Krichau, G. L.; Rieke, R. D. *Am. Chem. Soc. Div. Polym. Mater.: Sci. Eng.* **1995**, *73*, 66.

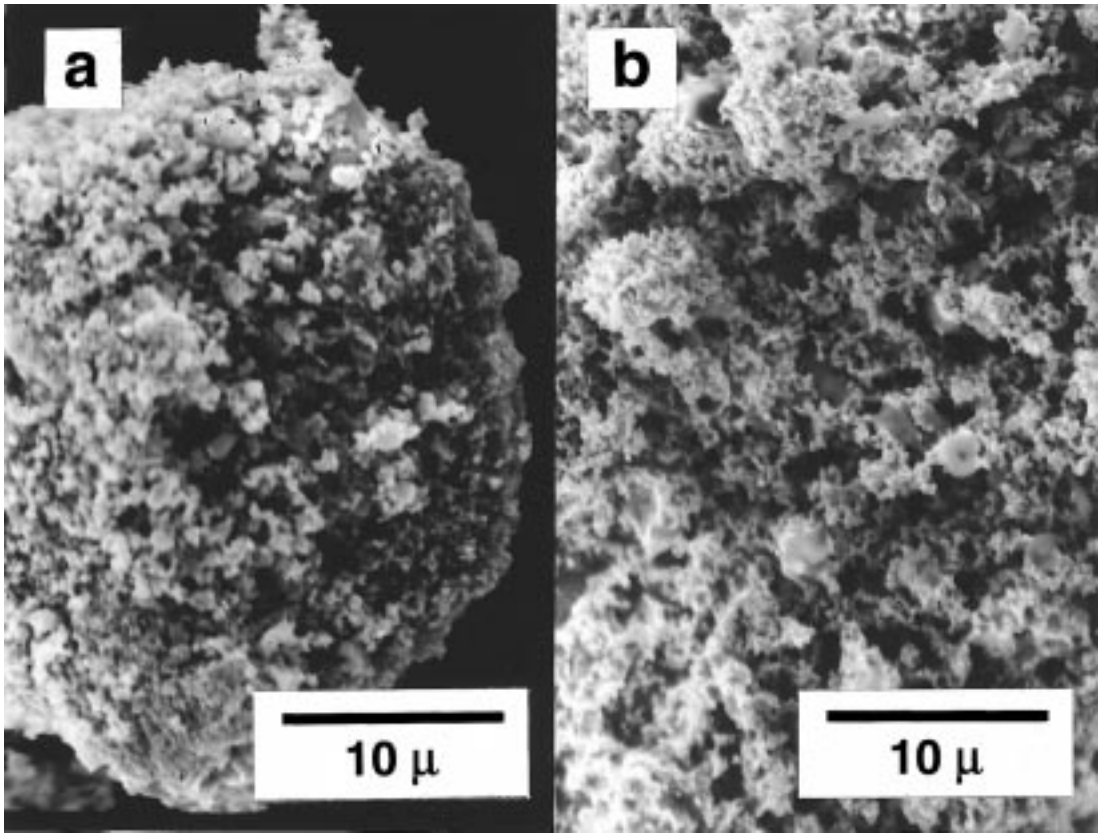

Figure 1. Scanning electron micrograph of nickel powders produced using eq 1 in (a) the as-synthesized state and (b) annealed. Note that both micrographs have the same length scale.

mercially purchased metals. The structure likely results from sintering of the precipitated powders and contributes to the enhanced reactivities relative to their commercial counterparts. The as-synthesized particles, shown in Figure 1a, have DCSs on the order of 3−5 nm, as determined by both X-ray diffraction and TEM; however, they agglomerate into much larger (0.1−1 μm) particles due to a combination of room-temperature sintering, electrostatic attraction, and magnetic attraction. Annealing produces an increase in both overall particle size and DCS. Figure 1b shows the SEM image of a sample annealed at 350 °C for 8 h. Since the chemical and magnetic properties of interest are often determined by the DCS and not the overall particle size, the DCS is a preferable parameter to enable the comparison of samples produced in different ways.

Energy dispersive X-ray analysis (EDX) shows that bromine is present in the particles. The relatively constant ratio of nickel to bromine at randomly sampled locations in unannealed material indicates that the bromine is not segregated. On annealing, segregation is observed: some regions are primarily nickel with little bromine present, and bromine-rich regions with a morphology very different than the nickel regions are observed. These regions can be quite large (10−20 μm) and do not exhibit the spongy appearance of the nickel particles, instead having larger (1 μm) crystallites that show distinct faceting. Small quantities of oxygen and silicon are observed. EDX shows no discernible differences between particles loaded into the SEM in a protective atmosphere and those loaded in air, so it is unlikely that the oxygen observed is introduced entirely during sample loading. The highly reactive particles

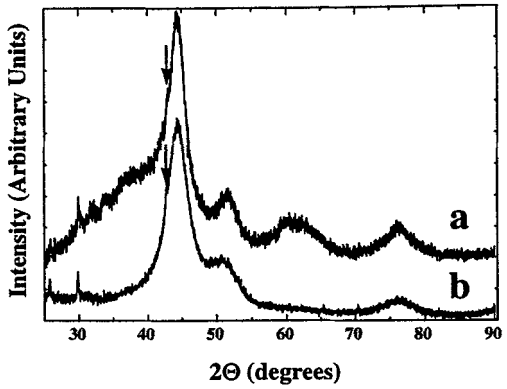

Figure 2. X-ray diffraction patterns for unannealed nickel made using eq 1. The pattern labeled a (run 38) is contrasted with the pattern labeled b (run 91). Run 91 was made with extreme care to eliminate adventitious oxygen and to ensure complete washing. The arrows indicate the position of a peak corresponding to carbon. Note that the peaks at 30.0° and 25.9° are present in both diffraction patterns.

may react with the Pyrex glass during annealing; however, a small amount of silicon is observed in the unannealed sample, suggesting that reaction with glassware during synthesis might also be a source of silicon.

Figure 2 compares the X-ray diffraction patterns for runs 38 and 91. Pattern a (run 38) shows diffraction peaks at the positions expected for nickel but also a number of impurity peaks at low angles. These peaks become more prominent as crystallites grow during annealing. The presence of these additional peaks led us to repeat the synthesis using exceptional care to eliminate adventitious oxygen throughout the synthesis (primarily by improving the cleanliness of the lithium

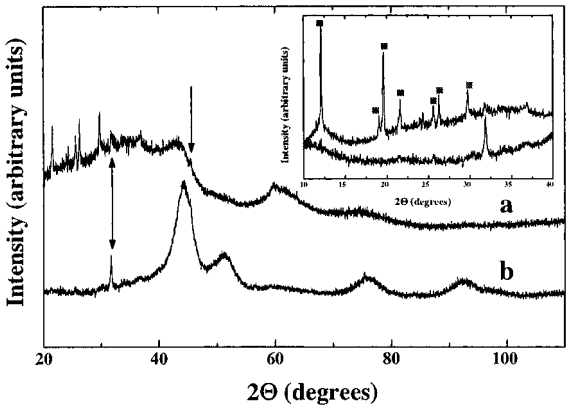

Figure 3. X-ray diffraction pattern of as-synthesized nickel powder before (upper) and after (lower) washing with THF. The solid squares in the inset represent naphthalene. The peaks at 31.7° and 45.5° are most likely carbon peaks.

used in the reaction and improving the integrity of the vacuum/argon line). The number of times the sample was washed was increased from five to seven times. The yield of this second run (denoted run 91 and shown as pattern b in Figure 2) is approximately 1.0, compared to the yield of 1.3 of run 38, which is consistent with improved removal of unwanted product.

The main characteristics of the diffraction patterns for the two as-synthesized materials are similar, with both having broad peaks indicating a nickel DCS of 3−5 nm. A shoulder at 42.8° on the primary nickel peak is identified as a form of carbon (JCPDS 26-1075) and becomes more evident as annealing sharpens the nickel diffraction peak. The improved washing eliminates some of the low-angle impurity peaks; however, both patterns show sharp peaks at 25.9° and 30.0° that persist to the highest annealing temperatures (500 °C). A number of compounds have a single strong diffraction peak at one of these two positions, making a positive identification difficult. Possibilities include Li_2NiO_2.

The most notable differences between the two samples are the broad shoulder on the left side of the most intense nickel peak (near 44°) and the broad peak near 62° seen in run 38 but not in run 91. The breadth of these features suggests that they are due to small particles formed during the reaction and not a crystalline compound residual from the starting materials. These peaks could be attributable to $Ni_3O_2(OH)_4$ and/or $Ni_2(OH)_2CO_3 \cdot C_4H_2O$. The lack of these features in the lower pattern is attributed to the improved washing protocol and/or the reduction of oxygen during the synthesis.

The effect of washing is confirmed by Figure 3, which compares the X-ray diffraction pattern from a nickel sample synthesized using $NiCl_2$ as the starting material before (a) and after (b) washing with THF. The inset shows the detail in the low-angle peaks, with naphthalene peaks indicated by solid squares. The broad peak near 62° is observed in the unwashed sample but is not present in the washed material. THF removes the naphthalene with minimal washing, but the peak at 62° is more resistant and requires repeated washings (five to seven times) to remove. Two distinct peaks remain in the washed material at 31.7° and at 45.4°. These two positions correspond to two of the most intense lines from a form of carbon (JCPDS 46-943) produced after

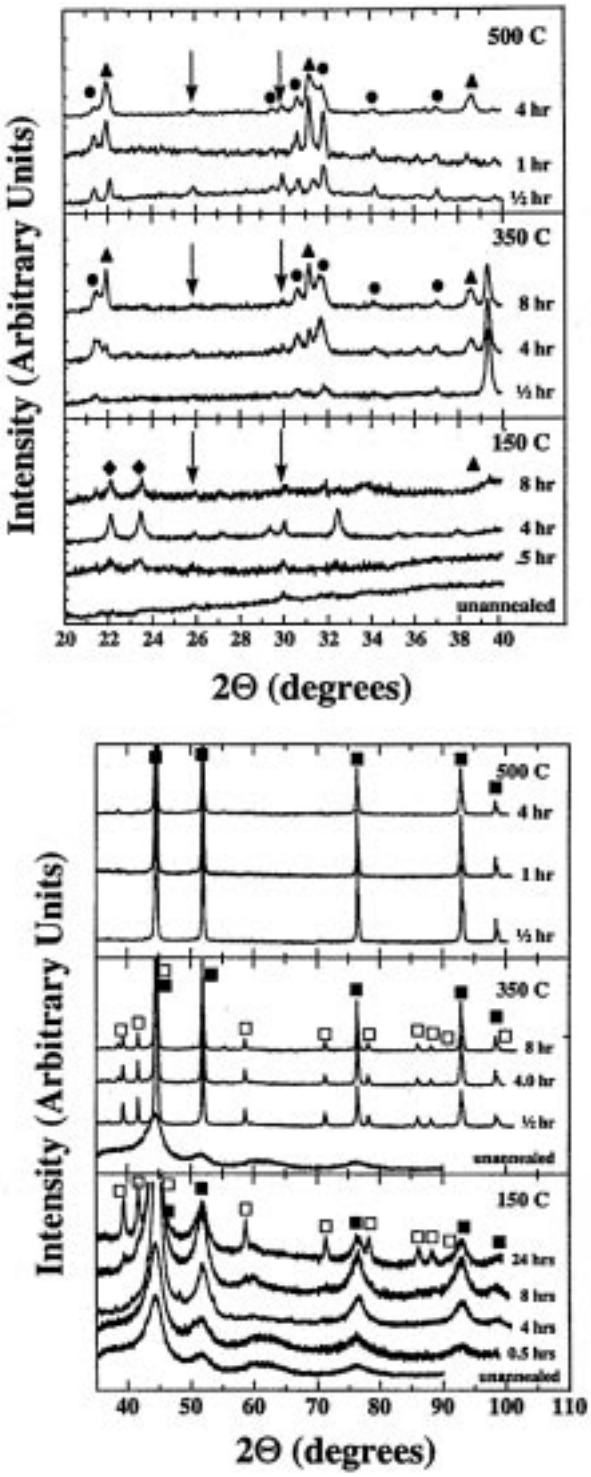

Figure 4. (a) Low-angle X-ray diffraction patterns from a series of samples from run 38 annealed at 150, 350, and 500 °C (bottom to top) for the times indicated. (b) High-angle XRD patterns from the same series of samples. In both figures, Li_2CO_3 is shown by solid circles, nickel by solid squares, Ni_3C by open squares, β-$LiBr \cdot H_2O$ or $Li_2(OH)Br$ by solid triangles and bromine acetate by solid diamonds.

heat treating at 1250 °C in the presence of nickel at very high (37 kbar) pressures.

Annealing. Samples are annealed at temperatures from 150 to 500 °C to investigate the growth of the crystallites and changes in chemical composition and/or structure. Figure 4 shows a series of XRD patterns from samples annealed at 150, 350, and 500 °C for times

ranging from 0.5 to 24 h. The low-angle detail is shown in Figure 4a, and the high-angle data are in Figure 4b.

Figure 4a shows that impurities remain after annealing. The peaks seen in the unannealed sample at 25.9° and 30.0° are present up to annealing temperatures of 500 °C, although they become weak in comparison to the other components. Lithium carbonate (Li_2CO_3) becomes evident in the annealed samples, probably formed due to the presence of active carbon. The presence of the lithium carbonate suggests that not all of the lithium in the reaction is participating in the reduction of the nickel bromide. Incomplete reduction could explain the observation of residual bromine by EDX.

The samples annealed at 150 °C show two low-angle peaks, indicated by diamonds, that are unidentified. The peak at 32.5° may be due to LiOH and disappears at temperatures above 200 °C. X-ray diffraction data at 350 and 500 °C show more clearly the presence of β-$LiBr{\cdot}H_2O$ and/or $Li_2(OH)Br$ (solid triangles) and $LiCO_3$ (solid circles). The presence of $LiBr{\cdot}H_2O$ and/or $Li_2(OH)Br$ up to the maximum annealing temperature is again attributed to incomplete washing of the sample. A preliminary investigation of differences between particles made using $NiCl_2$ or $NiBr_2$ shows that these impurities appear to be correlated to the starting salt. All of the syntheses made with $NiBr_2$ show sharp XRD peaks at 25.9° and 30.0°, whereas particles made using $NiCl_2$ do not show these peaks and instead exhibit a sharp XRD peak at 25.4°. Although this might suggest that the peaks are due to compounds containing either Cl or Br, the differences in reactivity of the particles made using each of these salts may affect solvent cleavage differently.

Examination of the high-angle diffraction patterns shows the expected nickel peaks, as indicated by solid squares in Figure 4, but also peaks indicating the presence of Ni_3C. The mechanisms leading to the formation of Ni_3C will be discussed later. Not shown in these diagrams is the continued presence of a peak at 42.8° on the left shoulder of the primary nickel peak due to a form of carbon (JCPDS 26-1075) and observed in a number of other samples. The presence of the nickel carbide and the carbon diffraction pattern signature is indicative of the cleavage of the solvent during synthesis and the subsequent crystallization during annealing.

As physical properties depend critically on the grain size, the growth of the DCS under different annealing conditions was investigated using eq 2. Figure 5 shows the dependence of the nickel and Ni_3C DCS on annealing time and temperature for run 38. Solid symbols represent the nickel DCS and open symbols the DCS of the nickel carbide. Solid lines are guides for the eye. For all temperatures, the majority of crystallite growth occurs during the first half hour of annealing, with subsequent growth being minimal. Ni_3C, which appears only between temperatures of 200 and 400 °C, is not detected with DCSs less than about 20 nm. The maximum DCS observed for both nickel and Ni_3C at the temperatures covered by this study is 50 nm. The relative amounts of nickel and Ni_3C range from infinite (no crystalline Ni_3C detected) to as low as 1.6, as shown in Table 1.

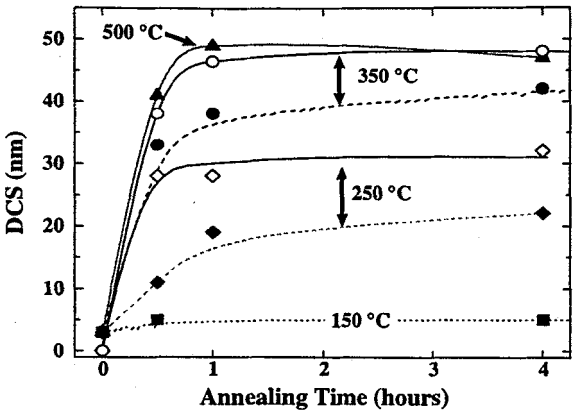

Figure 5. Dependence of the diffracting crystallite size (DCS) on annealing time for run 38. Solid symbols represent nickel and open symbols Ni_3C.

Table 1. Dependence of the Diffracting Crystallite Size (DCS) on the Annealing Time and Temperature for Run 38[a]

annealing conditions			DCS (nm)	
				ratio of areas
T (°C)	t (h)	Ni	Ni_3C	Ni:Ni_3C
unannealed		3		
150	0.5	5		
150	1	5		
150	4	5		
150	8	5		
150	24	5	20	4.3−5.5[a]
150	72	6	20	4.71
200	8	8	29	1.58
250	0.5	11	28	2.11
250	1	19	28	3.00
250	4	22	32	2.60
350	0.5	33	38	5.34
350	1	38	45	5.31
350	4	42	48	8.77
350	8	44	48	9.05
500	0.5	41		
500	1	49		
500	4	47		

[a] This peak was extremely broad and may include another peak. This range of figures represents the maximum and minimum values.

The XRD patterns for the samples of run 91—the more thoroughly washed material—are generally similar to those shown in Figure 4; however, neither $LiBr{\cdot}H_2O$ nor $Li_2(OH)Br$ diffraction peaks are observed due to the improved washing protocol. The presence of additional components in the material affects the nickel grain growth and the formation and growth of Ni_3C. Figure 6 shows the nickel and Ni_3C DCSs as functions of annealing temperature. The numbers shown under each point are the Ni:Ni_3C ratio as calculated by comparing the area under the peaks. The Ni:Ni_3C ratio is larger in the more thoroughly washed samples (run 91). Under identical annealing conditions, the nickel DCS of run 91 is consistently smaller than that of run 38. At 500 °C, the maximum nickel DCS is 50 nm for run 38 and 35 nm for run 91.

Formation of Ni_3C. In addition to a low maximum solubility of carbon in nickel (2.7 at. % at 1600 K), the metastable nature of Ni_3C can be attributed to a lack of ionic bonding and only loose covalent bonding.[38] The Boudard reaction,[39] in which an activated form of nickel metal reacts with carbon dioxide, produces Ni_3C but

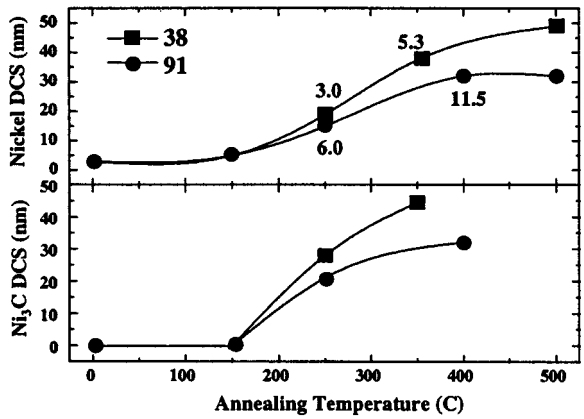

Figure 6. Comparison of the dependence of nickel and Ni_3C DCSs on annealing temperature for runs 38 and 91. All samples were annealed for 1 h. The numbers near each point denote the Ni:Ni_3C ratio.

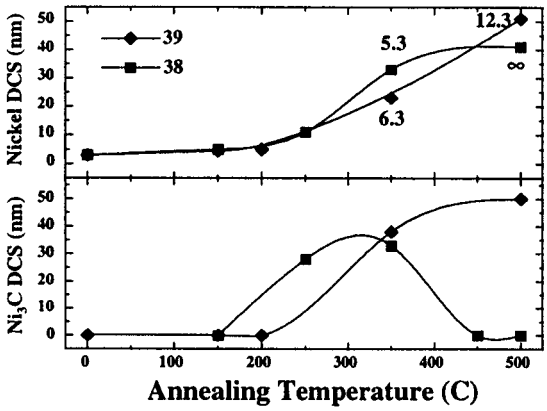

Figure 7. Comparison of the grain growth of Ni and Ni_3C as a function of temperature for samples with (run 39) and without (run 38) $P(Ph)_3$. All samples were annealed for 0.5 h. The numbers near each point denote the Ni:Ni_3C ratio.

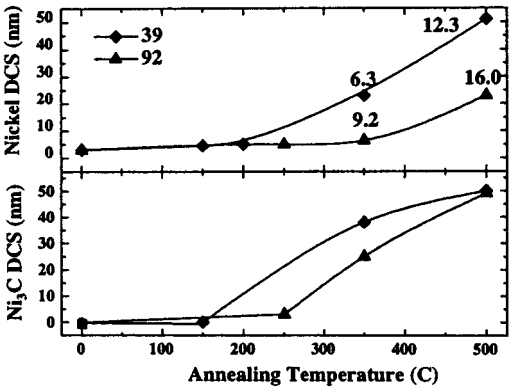

Figure 8. Comparison of the nickel and Ni_3C DCS for samples made with $P(Ph)_3$ added during synthesis (Run 39) or after synthesis (Run 92). All samples were annealed for 0.5 h.

requires high temperatures. Ni_3C can also be produced by the evaporation of nickel films on graphite,[38,40,41] metal vapor deposition,[20,21] and laser irradiation of nickel in a propane atmosphere.[42] Small particles having a large surface-to-volume ratio provide many reactive sites for dissociative chemisorption compared to polycrystalline materials; however, the sheer number of sites cannot be the only mechanism responsible for the formation of Ni_3C, as attempts to carburize activated nickel (at comparable temperatures) have been unsuccessful.[20,21] This suggests that not only highly reactive nickel—but also highly reactive carbon—are required for the formation of the carbide phase. The presence of elemental carbon has been confirmed by X-ray diffraction.

Ni_3C has a close-packed hexagonal structure and may be described by a hexagonal unit cell with lattice constants of $a_h = 2.682$ Å and $c_h = 4.306$ Å;[43] or a supercell with $a = \sqrt{3}a_h = 4.553$ Å and $c = 3c_h = 12.92$ Å.[44,45] The larger unit cell reflects the regular placement of carbon atoms in the octahedral interstices. The nickel octahedrons are slightly deformed, with the basal plane bonds being slightly longer than the other bond lengths.[46]

The formation of the carbide phase occurs via the adsorption of a C-containing molecule on the surface of a nickel cluster and subsequent decomposition of the adsorbed molecule during annealing. The carbon then diffuses into the nickel metal to form a carbide. The diffusive process, which occurs with a carbon diffusion coefficient in nickel in the range 10^{-10}–10^{-6} cm^2/s (873–1673 K),[47] depends on the presence of defects that can trap carbon atoms to nucleate the transition. Since carbon atoms diffuse more slowly through nickel carbide than through nickel, the initial carbide formation proceeds more rapidly than the formation of additional nickel carbide. The observation of graphite, mixed graphite/carbide and carbide, often observed is likely due to carbon atoms that cannot diffuse into the nickel particle and thus instead form a carbidic layer on the particle surface.[38,40,41,43] Graphitic carbide can also result by precipitation during the decomposition of nickel carbide.[48,49] Depending on other elements present and the breadth of the diffraction peaks, the carbon peaks may be observed in unannealed materials, as well as in the annealed samples made using eq 1.

Nickel carbide is produced from nickel metal in the relation $(001)_{Ni_3C}/(111)_{Ni}$, leaving the most densely packed planes in each metal parallel to each other. The transformation of nickel (which is fcc) into hcp Ni_3C occurs through a change in the stacking sequence due to dislocation motion on a slip plane.[38,40] The rate and temperature at which carburization occurs is strongly affected by the texture of the nickel metal, particularly in the carburization of films. The carburization process is diffusion-limited and increases with increasing temperature. Decomposition of Ni_3C occurs between 430 and 450 °C. In our materials, the peak intensity ratios for the Ni_3C do not correspond to those expected,

(38) Sinharoy, S.; Smith, M. A.; Levenson, L. L. *Surf. Sci.* **1978**, *72*, 710.
(39) Kuijpers, E. G.; Geus, J. W. *Fuel* **1983**, *62*, 159.
(40) Sinharoy, S.; Smith, M.; Levenson, L. L. *J. Vac. Sci. Technol* **1977**, *14*, 465.
(41) Sinharoy, S.; Levenson, L. L. *Thin Solid Films* **1978**, *53*, 31.
(42) Anisimov, V. N.; Baranov, V. Y.; Vladimirtseva, L. A.; Kopetskii, C. V.; Kraposhin, V. S.; Malyuta, D. D.; Pis'mennyi, V. D.; Sebrant, A. Y.; Shakhlevich, K. V. *Sov. Phys. Dokl. 3* **1986**, *1*, 505.
(43) Jacobson, B.; Westgren, A. *Z. Phys. Chem. B* **1933**, *20*, 361.
(44) Nagakura, S. *J. Phys. Soc. (Jpn.)* **1957**, *12*, 482–494.
(45) Baranova, R. V.; Khodyrev, Y. P.; Semiletov, S. A. *Sov. Phys. Crystallogr.* **198**, *27*, 554.
(46) Nagakura, S. *J. Phys. Soc. (Jpn.)* **1958**, *13*, 1005.
(47) Kovenskiy, I. I. *Phys. Met. Metallogr. (USSR)* **1963**, *16*, 107.
(48) Joyce, E. L.; Jervis, T. R. *Scrip. Met.* **1988**, *22*, 1313.
(49) Tebboth, J. A. *J. Soc. Chem. Ind.* **1948**, *67*, 62.

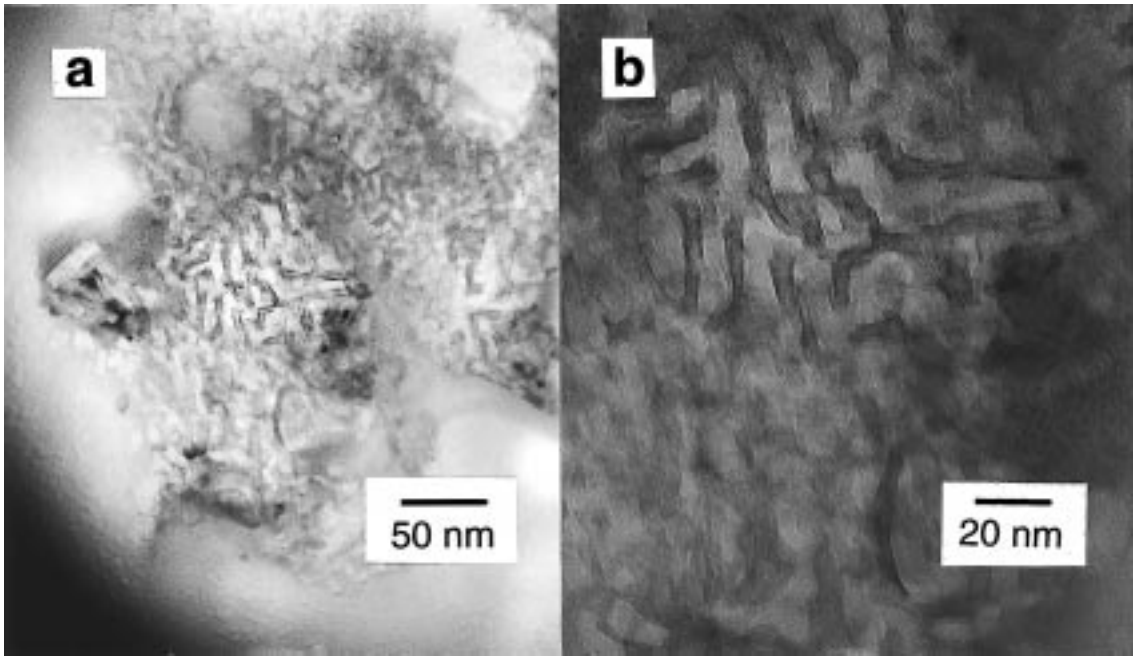

Figure 9. Transmission electron micrographs of Ni/Ni_3C nanocomposite annealed at 250 °C for 8 h.

although the nickel peaks are found with the correct intensity ratios. The reason for this is unclear at present. Preliminary electron diffraction measurements suggest that individual particles may have a preferential ordering in that the smaller grains comprising the particle share a common orientation.

We have not observed complete conversion of nickel into Ni_3C in these materials; however, coating the particles with MMA (methyl methacrylate), PMMA (poly(methyl methacrylate)), or polyacetylene prior to annealing has been found to assist the transformation.[20,21] The enhanced conversion is thought to be the result of reduction of NiO on the particle surface by the polymers. Surface NiO can block the diffusion of the carbon and may thus limit the transformation.

Effect of Surfactants. The addition of an appropriate surfactant during or immediately following synthesis can be used to affect the nucleation and growth of the particles. A proper choice of surfactant may also provide protection from oxidation. To investigate this effect, we fabricated powders using the reaction described by eq 1, but added triphenylphosphine ($P(Ph)_3$) during (run 39) or after (run 92) synthesis. The XRD pattern from the as-synthesized samples from run 39 was identical with that of run 38, including the sharp lines at 25.9° and 30.0°and the presence of $LiBr{\cdot}H_2O$ and/or $Li_2(OH)Br$ and Li_2CO_3. The presence of the surfactant affects both the growth of the nickel crystallites and the formation of Ni_3C, as demonstrated in Figure 7. The upper part of the figure shows that the nickel DCS behaves similarly in both materials; the slightly different behavior at higher temperatures may be attributable to the different proportions of Ni:Ni_3C. The presence of Ni_3C becomes evident at lower temperatures in run 38 than in run 39; however, at 500 °C, the Ni_3C had decomposed in run 38 but is still present in run 39. The presence of the $P(Ph)_3$ is evidently delaying the decomposition of the carbide phase until higher temperatures.

Persistence of Ni_3C to higher temperatures is also found in run 92, in which the triphenylphosphine was added after the particles had precipitated. The XRD pattern of the as-synthesized particles from run 92 is again identical to that of run 91, made without $P(Ph)_3$. When the surfactant is added during synthesis, the progression of nickel crystallite growth is very similar to that observed in samples without surfactant; however, when the surfactant is added postsynthesis, growth of the nickel crystallites is significantly retarded, as shown in Figure 8. A nickel DCS of 6−8 nm is retained up to an annealing temperature of 350 °C, whereas a similarly annealed material without the triphenylphosphine has a nickel DCS of 24 nm. After annealing at 500 °C for 8 h, the samples with the triphenylphosphine have a nickel DCS of 23 nm as compared with 35 nm in the samples without the triphenylphosphine. In samples where the surfactant is added after synthesis, broad Ni_3C peaks are evident after annealing at temperatures as low as 150 °C and times of 1 h, whereas they are not observed in the samples coated during synthesis until they are annealed at temperatures of at least 250 °C. These preliminary results show that surfactants can be used to modify the temperature dependence of the nickel crystallite growth, as well as the growth and subsequent decomposition of the carbide phase. In general, the Ni:Ni_3C ratio is greater in samples with a surfactant than those without, in contrast to the effects of MMA or PMMA coating as discussed earlier. The most likely mechanisms are the direct formation of a diffusion barrier preventing carbon from diffusing into the nickel, or prevention of the reduction of nickel oxides on the surface that can also form a diffusion barrier.

The unique behavior of the postsynthesis coated particles is illustrated by a strong correlation between Ni DCS and Ni_3C DCS in all runs except run 92. In the regime where both Ni and Ni_3C are present, the DCSs are related roughly linearly. The different behavior of run 92, where no type of correlation is

observed, is likely due to the presence of the PPh_3 as a coating layer added after the particles had already been formed.

Figure 9 shows transmission electron micrographs of a nickel/nickel carbide nanocomposite material from run 38 annealed at 250 °C for 2 h. The morphology is very similar to that observed in nanocrystalline Ni_3P/Ni made by annealing amorphous $Ni_{80}P_{20}$,[24,50] including some degree of orientation of the square crystallites. Although the growth mechanism in the Ni_3P system is different due to Ni_3P being an equilibrium phase, the cluster shear model, in which small correlated clusters change their orientation in the presence of a growing crystal front, may also be applicable to our materials and might explain electron diffraction measurements showing preferential crystal orientation. Differential broadening of the XRD peaks due to Ni_3C is observed, suggesting the possibility of slightly anisotropic crystal shape. No differential broadening is observed in the nickel XRD peaks.

Conclusions

We have demonstrated that the Rieke technique as described by eq 1 can be used to produce nickel-based nanocomposites with diffracting crystallite sizes from 3 to approximately 50 nm. The high reactivity of the nickel particles formed causes the incorporation of hydrocarbon fragments in the particles. Thorough washing is necessary to remove byproducts of the reaction, although retention of these byproducts can in some cases be advantageous due to modification of the crystallite growth behavior on annealing and the possibility of fabricating materials with in situ getters. Regardless of postsynthesis washing, all of the samples produce the metastable Ni_3C phase upon annealing. The addition of $P(Ph)_3$ either during or immediately after synthesis modifies the growth of the nickel crystallites with annealing time and temperature. The presence of the surfactant can also significantly affect the temperature at which Ni_3C crystallites are first formed and promote their retention at temperatures higher than the usual decomposition temperature of 430 °C. Additional components, such as Li_2CO_3, may be present in the unannealed materials and become more evident in annealed samples due to increased crystallinity.

Acknowledgment. The authors gratefully acknowledge partial financial support by the National Science Foundation (via OSR9553350 and OSR925525) and the University of Nebraska's Center for Materials Research & Analysis. We especially thank Gary Krichau of the CMRA Central Facility for Electron Microscopy for taking the transmission electron micrographs shown in Figure 9.

CM9702979

(50) Sui, M. L.; Lu, K.; He, Y. Z. *Philos. Magn. B* **1991**, *63*, 993–1008.